# Static and Dynamic Scaling Relationships in the Light Scattering Properties of Polystyrenes in Good Solvents

**Mamta Bhatt,[†] Alex M. Jamieson,*[,†] and Rolfe G. Petschek[‡]**

*Departments of Macromolecular Science and Physics, Case Western Reserve University, Cleveland, Ohio 44106.* *Received July 13, 1988; Revised Manuscript Received September 19, 1988*

ABSTRACT: Static light scattering measurements are reported on narrow molecular weight distribution polystyrenes ($M_w = 3.84 \times 10^6$) in the four good solvents, ethylbenzene, benzene, toluene, and tetrahydrofuran at 25 °C. These data are plotted in a "scaling" form to directly compare the equilibrium structure factor of identical polystyrene samples in the different solvent systems. The results in tetrahydrofuran are clearly distinct from those in the aromatic solvents and apparently suggest that THF is a thermodynamically better solvent. These distinctions between our results for identical, high molecular weight polymer samples in different good solvents demonstrate that these molecular weights are not high enough to be in the asymptotic good solvent limit (at least not in both solvents), so that current experimental values of universal ratios in this limit are not reliable. We also compare dynamic light scattering characteristics of polystyrene samples ($M_w = 8.42 \times 10^6$ and $20 \times 10^6$) in ethylbenzene and in tetrahydrofuran over the small to intermediate $qR_g$ region. For $qR_g < 1.0$, we obtain the infinite dilution translational diffusion coefficient $\langle D_t \rangle_z^0$ and at $qR_g > 1.0$, we determine the dimensionless decay rate $\Gamma^* = \Gamma_e(q,c)/(q^3kT/\eta_0)$, where $\Gamma_e$ is the first cumulant of the decay function. The values, $\Gamma^*(q)$, characteristic of a single coil, have been obtained by extrapolating $\Gamma_e$ to $c = 0$. As predicted by theory, the reduced quantity $\Gamma^*(q)$ slowly approaches a constant asymptote at $qR_g \gg 1.0$. We show that an accurate determination of the asymptote can be obtained from a plot of $\Gamma^*(q)$ versus $(qR_g)^{-2}$. The asymptotic value obtained for polystyrene chains in ethylbenzene is significantly different, about 15% smaller than that determined for polystyrene in tetrahydrofuran. This indicates differences in the internal coil hydrodynamics of polystyrene in these two chemically dissimilar good solvents.

## Introduction

Static and dynamic light scattering experiments by many different groups have focused on polystyrene (PS) chains of narrow molecular weight distribution in good, marginal, and Θ solvents. These data have been compared with theoretical models for the configurational and hydrodynamic properties of linear flexible chains. In our laboratory we have carried out light scattering measurements on polystyrene in the good solvents—ethylbenzene (ETBZ)[1] and tetrahydrofuran (THF).[1,2] We observed similar radii of gyration, $R_{g,z}$, for polystyrene in each of these solvent systems, comparable to values independently reported for PS in benzene (BZ)[4-6] and toluene (TOL).[7,8] These observations suggest similar solvating powers for polystyrene in all four solvents. On the other hand, values of the second virial coefficient, $A_2$, were found[1,2] to be significantly larger for PS in tetrahydrofuran than in the aromatic good solvents.[4-8] Also, hydrodynamic radii, $R_h$, measured for PS in THF[1-3,9-12] are 15% larger than those reported in ethylbenzene,[3] benzene,[5] and toluene.[8] Hence, comparison of the universal ratios

$$\psi = A_2M^2/4\pi^{3/2}N_A\langle R_g^2\rangle^{3/2} \quad (1)$$

and

$$U_{fs} = 6\pi R_h/\langle R_g^2\rangle^{1/2} \quad (2)$$

for PS in the various solvent systems shows that the values for PS in THF are substantially different from those in the aromatic good solvents. For example, we determined[1,2] $\psi = 0.315 \pm 0.03$ for PS in THF[2] and $\psi = 0.211 \pm 0.02$ for five PS samples in the molecular weight range $0.9 \times 10^6 \leq M_w \leq 8.42 \times 10^6$. In addition, the average values of $U_{fs}$ were determined to be $U_{fs} = 14.7 \pm 0.1$ for PS/THF and $U_{fs} = 11.8 \pm 0.08$ for PS/ETBZ. These results pose some problems since previous interpretations[19] have suggested that PS in benzene is already at the nondraining good solvent limit when the molecular weight is greater than $\sim 10^5$. Thus, theory predicts[18,22] that $\psi$ should increase monotonically with an increase in solvent quality and should reach a constant asymptotic value $\psi_\infty = 0.269$ for very good solvents. Thus we might conclude from the larger values of $\psi$ for PS in THF that it is a better solvent for polystyrene than ETBZ. As a cautionary note, however, the possibility of nonuniversal behavior in the $\psi$-function has been previously suggested, based on both theoretical[48,49] and experimental results.[50,51]

Likewise, differences in the values of $U_{fs}$ for PS/THF and PS/ETBZ are of considerable interest since values of $U_{fs}$ are predicted[18-23] to exhibit universal behavior for polymer–solvent systems in the crossover from the Θ to the good-solvent asymptote, provided the strength of the hydrodynamic interaction is constant. There is, however, disagreement as to the precise nature of the crossover function. For example, the renormalization group (RG) theory analysis of Oono and Kohmoto[18] predicts that for nondraining chains, $U_{fs}$ decreases from a value of approximately 14 at the Θ condition to a value of approximately 12 in the good-solvent limit. Thus, our values of $U_{fs}$ for PS in ethylbenzene are in agreement with the Oono–Kohmoto[18] prediction while the values of $U_{fs}$ for PS in THF are substantially different. An independent RG analysis by Douglas and Freed[22,23] arrives at the very different conclusion that $U_{fs}$ is essentially independent of excluded volume and can vary only if the nature of the hydrodynamic interaction changes. From this viewpoint, changes in $U_{fs}$ are attributed either to draining effects[22,23] or to a decrease in the strength of internal friction[21] with chain expansion. Since PS/THF and PS/ETBZ are both good-solvent systems, the differences which are observed in the values of the ratio, $U_{fs}$, for PS in THF versus ETBZ seem to indicate that there are differences in the nature of the internal chain hydrodynamics in these solvent systems.

In this paper, we further explore the differences in thermodynamic behavior between PS in aromatic good solvents and in THF, by comparing directly the static light scattering intensity data for identical polystyrene samples in these different solvent systems. In addition, we extend

[†] Department of Macromolecular Science.
[‡] Department of Physics.

0024-9297/89/2222-1374$01.50/0 

analysis of the dynamic light scattering data to large scattering vectors ($qR_g \gg 1.0$) to compare the intramolecular dynamical behavior of a single polystyrene chain in THF and ETBZ. This is accomplished by determining the effective decay rate, $\Gamma_e$, of the photon correlation function and by comparing the reduced quantity $\Gamma^*(q) = \lim_{c=0} \Gamma_e(q)\eta_0/kTq^3$ as a direct measure of differences in the chain hydrodynamics for PS in THF versus the aromatic good solvents.

## Experimental Section

**Materials.** Narrow distribution PS standards were obtained from Pressure Chemicals (Pittsburgh) and were used without further purification. The weight-average molecular weights used were $3.84 \times 10^6$, $8.42 \times 10^6$, and $20 \times 10^6$. All samples were characterized by methods of static light scattering in our laboratory and in each case the molecular weights were reproduced to within a few percent of their specified values.[2] The solvents, tetrahydrofuran (THF), ethylbenzene (ETBZ), benzene (BZ), and toluene (TOL) were obtained from Aldrich Chemical Co. as ACS spectrograde quality solvents. Due to its hygroscopic[25] nature THF was further distilled with $LiAlH_4$ and refluxed in a dry inert atmosphere prior to use. All the other solvents were used without further purification.

**Physical Properties.** The refractive indices of the solvents were measured at 25 °C in an Abbe Refractometer (Series 361-XU) and were determined to be $n_{THF} = 1.407$, $n_{ETBZ} = 1.495$, $n_{TOL} = 1.494$, and $n_{BZ} = 1.498$. The specific refractive index increment, $dn/dc$, of PS in the various solvents was determined by using a Brice Phoenix differential refractometer at 6328 Å and was obtained to be $dn/dc_{THF} = 0.192$ cm$^3$/g, $dn/dc_{ETBZ} = 0.111$ cm$^3$/g, $dn/dc_{TOL} = 0.105$ cm$^3$/g, $dn/dc_{BZ} = 0.106$ cm$^3$/g at 25 °C. The viscosities of ethylbenzene and tetrahydrofuran were measured at 25 °C by using a Cannon Ubbelohde viscometer which was calibrated by other solvents. The flow times were selected to ensure that kinetic energy corrections were negligible. The viscosities of ETBZ and THF at 25 °C were determined to be 0.619 cP and 0.465 cP, respectively.

**Sample Preparation.** Dilute solutions of PS in the different solvents were made by weighing individual samples in a Perkin-Elmer microbalance, Model AD-2, with an accuracy of ±0.01 mg. The method of sample dissolution and preparation has been described elsewhere in detail.[2] All solutions were checked for optical clarity by monitoring the scattered intensity for 80–100 runs of 1-s duration each and only those solutions were used where the fluctuations in the scattered intensity were less than ±2%. This ascertained the absence of dust particles or other nonhomogenieties which are sources of parasitic scattering and prevent a meaningful interpretation of the time correlation function. All experiments were repeated after a period of several days and the measurements were found to be within 2% of each other.

**Methods.** All scattering experiments were performed on a Brookhaven Instrument Corp. spectrometer comprising a BI 240 goniometer and a BI 2030 AT correlator with a SpectraPhysics 15-mW He/Ne laser ($\lambda = 6328$ Å). Cylindrical sample cells were used and mounted at the center of a temperature controlled, refractive index matched bath. Temperatures were controlled at 25 ± 0.1 °C for all experiments. Absolute calibration of the spectrometer was made with benzene (Spectro-grade, Aldrich Chemicals) for which the absolute Rayleigh ratio at $\lambda = 6328$ Å was assumed to be $R_{V,V+H}(90) = 11.84 \times 10^{-6}$ as reported by Pike et al.[32] All measurements were made from 20–120° scattering angles. For dynamic measurements the intensity autocorrelation function was measured on a 264-channel BI 2030 AT 4-bit correlator with a multiple sampling time option. In addition, eight delay channels were used to determine the measured baseline for a given autocorrelation function. To probe relaxation processes occurring on widely differing time scales, multiple sampling times were used to obtain the correlation function. For this, the 264 real time channels in the correlator were split into four successive groups of 64 channels each and the eight delay channels were added to the last group. The sample time for each group could then be selected as a power of 2 times the base sample time, $\tau_1$, employed for the first group. Hence, the first group consists of 64 equally spaced sample times, $\tau_1$, and the successive groups could have a sample time, $\tau_{i+1} = \tau_i \times 2^n$ where $i = 1, 2, 3, 4$ and $n = 0, 1, 2, 3, ..., 8$. This multiple sampling time option allowed us to obtain information about different parts of the relaxation spectrum simultaneously resulting in an accurate determination of the form of the line-width distribution function, $G(\Gamma)$. Only those intensity–intensity time correlation functions, $C(\tau)$, where the difference between the calculated and measured baselines was less than 0.1% were used for data analysis. Dynamic measurements were repeated at least twice to check for reproducibility and were found to be within 2–4% of each other. The data were further analyzed on an IBM/AT computer and a VAX 11/780.

**A. Static Measurements.** The excess Rayleigh ratio due to concentration fluctuations is obtained from the absolute excess scattered intensity and for vertically polarized incident light is reported theoretically to approximate[26]

$$\frac{Kc}{R(\theta)} = \frac{1}{M_w P(\theta)} + 2A_2c + 3A_3c^2 + ... \tag{3}$$

where $K = 4\pi^2 n_0^2 (dn/dc)^2 / N_A \lambda^4$ and $A_2$ and $A_3$ are the second and third osmotic virial coefficients, respectively. $n_0$ is the refractive index of the solvent, $N_A$ is Avogadro's number, $c$ is the concentration in g/mL, and $\theta$ is the scattering angle. $P(\theta)$, the particle scattering function, can be expressed as

$$P^{-1}(\theta) = \left[1 + \frac{16\pi^2 n_0^2 \langle R_g^2 \rangle \sin^2(\theta/2)}{3\lambda^2} + ...\right] \tag{4}$$

Equation 3 in the limit of zero angle and infinite dilution yields

$$\lim_{\substack{c\to 0 \\ \theta \to 0}} \frac{Kc}{\Delta R(\theta)} = \frac{1}{M_w} \tag{5}$$

Static measurements were performed over a range of concentrations and scattering angles. The Zimm[26] plots exhibited noticeable curvature due to a finite third virial coefficient, and hence square-root plots[27] were used to determine the molecular weights. Thus a plot of $(Kc/\Delta R(\theta))_{\theta \to 0}^{1/2}$ versus $c$ was used to determine $A_2$, and $\langle R_g^2 \rangle_z^{1/2}$ was obtained from the slope of $(Kc/\Delta R(\theta))_{c \to 0}^{1/2}$ versus $\sin^2(\theta/2)$. For $M_w = 20 \times 10^6$ it was necessary to generate a Fujita[53] plot to obtain an accurate estimate of the molecular weight.

**B. Dynamic Measurements.** Dynamic measurements were performed on the polymer samples of $M_w = 8.42 \times 10^6$ and $20 \times 10^6$ coded as L-1 and L-2. The quantities determined were the average line width, $\Gamma_e$, the $z$-average translational diffusion coefficient, $\langle D_t^0 \rangle_z$, and the corresponding Stokes radius, $R_h$. The average decay rate, $\Gamma_e$, and the variance $\mu_2/\Gamma_e^2$ are related[14] to the normalized distribution function, $G(\Gamma)$, of relaxation time constants $\Gamma = D_t q^2$

$$\Gamma_e = \int_0^\infty G(\Gamma)\Gamma \, d\Gamma \tag{6}$$

$$\mu_2 = \int_0^\infty (\Gamma - \Gamma_e)^2 G(\Gamma) \, d\Gamma \tag{7}$$

with

$$\int G(\Gamma) \, d\Gamma = 1 \tag{8}$$

The experimental intensity–intensity correlation function $G^2(\tau)$ is related to $G(\Gamma)$ by

$$G^2(\tau) = A(1 + b|g^1(\tau)|^2) \tag{9}$$

$$|g^1(\tau)| = \int_0^\infty G(\Gamma) \exp(-\tau\Gamma) \, d\Gamma \tag{10}$$

where $A$ is the background (or the base line), $b$ is a constant which is a function of the detecting optics and accounts for the nonideal point detector, and $|g^1(\tau)|$ is the normalized electric field autocorrelation function. Following the analysis of Koppel,[14] $|g^1(\tau)|$ can be expanded in a Taylor series

$$|g^1(\tau)| = \exp(-\Gamma_e\tau)\{1 + (\Gamma - \Gamma_e)^2\tau^2/2! + ...\} \tag{11}$$

and a polynomial expansion of $\ln g^1(\tau)$ leads to

$$\ln |g^1(\tau)| = -\Gamma_e\tau + \frac{\mu_2(\Gamma_e\tau)^2}{\Gamma_e^2(2!)} - ... \tag{12}$$

where the zeroth order moment $\Gamma_e$ is related to the $z$-average translational diffusion coefficient $\langle D_t \rangle_z$ by

$$\Gamma_e = \langle D_t \rangle_z q^2 \tag{13}$$

where $q = 4\pi n_0 \sin(\theta/2)/\lambda$.

For the intermediate $qR_g$ region, where $qR_g > 1$, the second-order cumulant fit proves inadequate. This occurs because the correlation function becomes increasingly nonexponential due to contributions from configurational motions and multimodal line-width distributions are obtained. Therefore, alternative methods of analysis must be used which involve obtaining an estimate of $G(\Gamma)$, the line-width distribution function. In principle, $G(\Gamma)$ can be obtained by inversion of the Laplace transform in eq 10. However, in practice, the correlation function contains noise, and Laplace inversion then becomes a very difficult ill-conditioned problem. Thus, several approximation procedures[28-41] have been developed and used to obtain the form of $G(\Gamma)$.

For our experiments in the intermediate $qR_g$ region, the data have been analyzed by using a Pike–Ostrowsky multiexponential (MEXP) sampling method[28-31]. This technique approximates $G(\Gamma)$ by a set of logarithmically or linearly spaced discrete single exponentials

$$G(\Gamma) = \sum_j P_j \delta(\Gamma - \Gamma_j) \tag{14}$$

where $P_j$ are the weighting factors of the $\delta$ function and

$$\sum_j P_j = 1 \qquad \text{(normalization condition)}$$

$$\Gamma_j/\Gamma_{j-1} = K \qquad (K = \text{constant})$$

Substituting for $G(\Gamma)$ in eq 10 yields

$$|g^1(\tau)| = \sum_j P_j \exp(-\Gamma_j \tau) \tag{15}$$

where each of the $P_j$ contributions is linearly independent. Following the procedure of Ostrowsky et al.[28,29] the correlation function is sampled at a series of linearly or exponentially spaced sample times. Then, it has been shown[28] that the Nyquist sampling theorem can be applied along with an interpolation procedure[29] to fully reconstruct the correlation function at all values of $\tau$ limited only by the band-limit $\omega_{max}$. The experimental noise in the $G^2(\tau)$ data defines $\omega_{max}$, which is a relative measure of the resolution of the obtained fit, i.e., $G(\Gamma)$ cannot be resolved at points closer than $\pi/\omega_{max}$. Hence, the higher the value of $\omega_{max}$ the better the resolution in $G(\Gamma)$. Then a linear least squares procedure is used where

$$\sum_{i=1}^{M} (G^2(\tau) - \sum_{n=1}^{N} a_n \exp(-\Gamma_i \tau))^2 \tag{16}$$

is minimized and a semilog plot of $a_n$ versus $\Gamma$ is obtained. The values of the average decay rate, $\Gamma_e$, determined from the above analysis are obtained with high precision. The computed fits to the experimental data $G^2(\tau)$ can be assessed from plots of the residuals

$$\frac{G^2(\tau) - G^2(\tau)_c}{G^2(\tau)} \tag{17}$$

where $G^2(\tau)_c$ is the obtained fit. Figure 1A gives an example of a normalized autocorrelation function obtained for a solution of the highest molecular weight sample (L-2) in ETBZ with $c = 0.19 \times 10^{-3}$ g/cm$^3$ at a scattering angle of $\theta = 50°$. Figure 1B,C shows the result of a multiexponential fit on this data together with a plot of the corresponding residuals. In a separate report we discuss the interpretation of the bimodal shape of the $G(\Gamma)$ function. Here we focus on the behavior of $\Gamma_e$ in the intermediate $q$ vector region ($qR_g \geq 1.0$).

## Results

**Static Properties.** Static intensity data were obtained for a sample of $M_w = 3.84 \times 10^6$ in the solvents benzene, ethylbenzene, toluene, and tetrahydrofuran at 25 °C. The results of the static measurements are listed in Table I, together with the computed values of the interpenetration parameter $\psi$. The molecular weights are identical within experimental error and are in good agreement with suppliers specifications. The radii of gyration and the second virial coefficients are in good agreement with data reported previously in the literature. As is evident, there are small systematic differences in $A_2$, $M_w$, and $R_{g,z}$ which combine to make $\psi$(THF) > $\psi$(BZ) ~ $\psi$(TOL) > $\psi$(ETBZ). These systematic variations are comparable to the experimental errors on the quoted quantities but have been repeatedly observed on polystyrene samples of different molecular weights. To exhibit these differences more directly, in Figure 2 we graph $KcM_w/\Delta R_\theta(q,c)$ against $q^2 + kc^{2/3}$ where $K$ is an optical constant, $R$ is the Rayleigh ratio, $q$ is the scattering wavevector, $c$ is the concentration, and $k$ is an arbitrary constant. This plot, in which the $c$- and $q$-dependence of the scattered intensity is compared against a single length scale, is a test of universality which avoids the extrapolations and graphical analyses which are a significant source of error in the evaluation of $\psi$. Both scaling theory and the renormalization group predict that, with a possible change of length scale, corresponding to a change in polymer microstructure, such plots for identical polymer samples should superpose provided (a) the solvents are good enough and (b) the molecular weight of the polymer is high enough (and the distribution of molecular weights is not very broad) so that the asymptotic good solvent limit has been reached. As Figure 2 shows, the intensity data for polystyrene in tetrahydrofuran increase

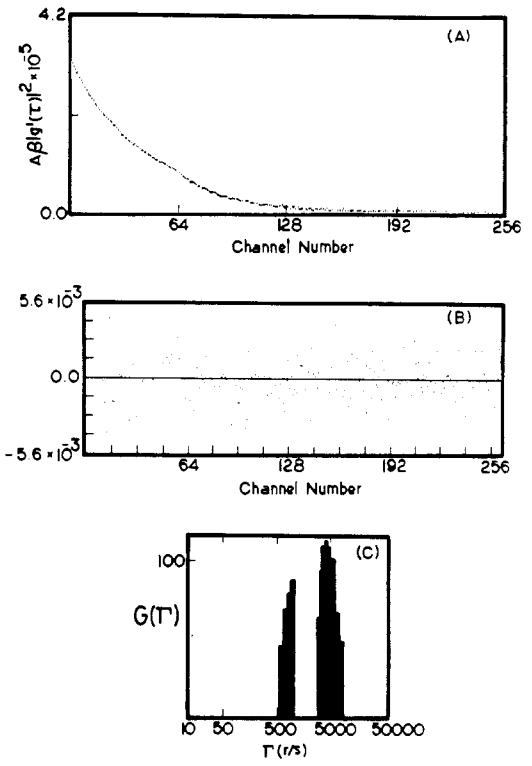


**Figure 1.** (A) Example of a normalized correlation function for the solution of the highest molecular weight sample (L-2) in ETBZ with $c = 0.19 \times 10^{-3}$ g cm$^{-3}$ at $\theta = 50°$ and $\tau_1 = \tau_2 = 35$ μs, $\tau_3 = 70$ μs, and $\tau_4 = 140$ μs. (B) Plot of the residuals versus channel number. (C) The corresponding distribution for $G(\Gamma)$ versus $\Gamma$.

**Table I**
**Static Light Scattering Characteristics of Polystyrene in Good Solvents**

| | $10^6 M_w \pm 5\%$ | $R_{g,z} \pm 5\%$, Å | $10^{-3}A_2 \pm 8\%$, mol cm$^3$ g$^{-2}$ | $\psi \pm 14\%$ |
|---|---|---|---|---|
| PS-BZ | 3.71 | 937 | 0.201 | 0.271 |
| PS-TOL | 3.72 | 936 | 0.196 | 0.247 |
| PS-ETBZ | 3.71 | 925 | 0.174 | 0.226 |
| PS-THF | 3.77 | 915 | 0.219 | 0.316 |

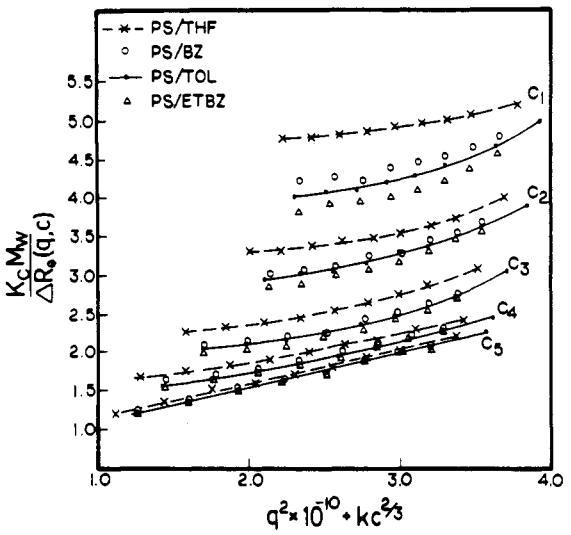


**Figure 2.** Plot of $KcM_w/\Delta R_\theta(q,c)$ versus $q^2 \times 10^{-10} + kc^{2/3}$ for PS ($M_w = 3.84 \times 10^6$) in THF (×), ETBZ (△), TOL (●), and BZ (○).

more rapidly with concentration than the corresponding data for benzene, toluene, and ethylbenzene. This implies that the osmotic compressibility in THF is larger than in the aromatic good solvents, consistent with our experimental determination of larger second virial coefficients in the PS–THF system. It is further pertinent to note that the data for PS in all the solvent systems superposes at low concentrations indicating comparable values of the radii of gyration, $R_{g,z}$. Figure 2 demonstrates that it is impossible to superpose all of the intensity data by a simple expansion of the horizontal length scale. This indicates that the differences in light-scattering properties cannot be explained due to solely a change in polymer microstructure (conformation). Thus we conclude that there are indeed substantial differences in the solvating power of these different solvents for atactic polystyrene, consistent with the reported experimental values of $\psi$; it appears that the order of solvation power is THF ≫ BZ ~ TOL > ETBZ.

It is of further interest to plot our static data in a universal scaling form suggested by Wiltzius et al.,[17] based on theory of Ohta and Oona.[54] They found that the quantities $(\xi/R_g)$ and $(M_w/RT)(\delta\pi/\delta c)$ are universal functions of $X = (16/9)A_2M_wc$, where $\xi$ is the spatial correlation length at a finite concentration and $(\delta\pi/\delta c)$ is the osmotic compressibility and hence

$$Kc/\Delta R_\theta = (1/RT)(\delta\pi/\delta c)[1 + (\xi q)^2 + (\xi q)^4 + ...] \quad (18)$$

In Figure 3 and 4 we show that our experimental data for the quantities $(\xi/R_g)$ and $(M_w/RT)(\delta\pi/\delta c)$, when plotted versus $X$, superpose quite well, in good agreement with the observations of Wiltzius et al.[17] Thus, for THF, which has the largest value of $A_2$, $\xi$ decreases with concentration more rapidly than for the aromatic solvents. This observation appears to correspond essentially to a self-consistency check on the light scattering data as can be shown by comparing the theoretical description of eq 18 with that[26,52] of eq 3. Thus, in the regime $qR_g \ll 1$, eq 3 leads to

$$\frac{Kc}{\Delta R_\theta} = \frac{1}{M_w}\frac{q^2R_g^2}{3} + \frac{1}{RT}\left(\frac{\partial\pi}{\partial c}\right)^{-1} \quad (19)$$

Comparing eq 18 and 19 we deduce

$$\frac{\xi^2}{R_g^2} = \frac{RT}{3M_w}\left(\frac{\partial\pi}{\partial c}\right)^{-1} \quad (20)$$

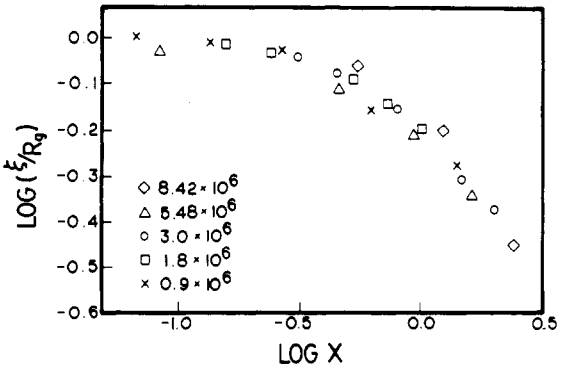


**Figure 3.** Universal plot of log $(\xi/R_g)$ versus log $X$ as suggested by Wiltzius et al.[17]

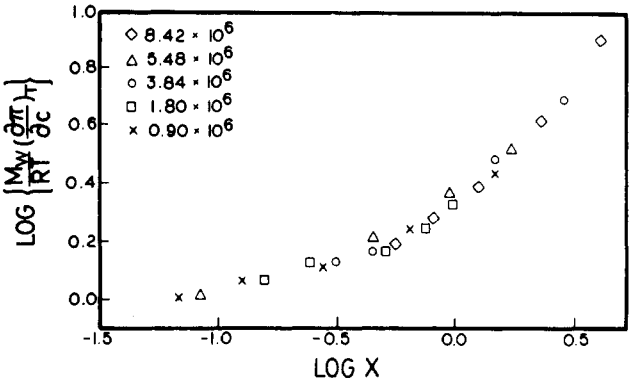


**Figure 4.** Universal plot of log $M/RT(\delta\pi/\delta c)$ versus log $X$ as suggested by Wiltzius et al.[17] (Symbols have the same meaning as in Figure 3.) Shown are the data for PS in THF: (×) $0.9 \times 10^6$; (□) $1.8 \times 10^6$; (○) $3.84 \times 10^6$; (△) $5.84 \times 10^6$; (◇) $8.42 \times 10^6$.

a result consistent with the experimental observations (Figures 3 and 4).

**Dynamic Properties.** We have determined the infinite dilution translational diffusion coefficients $D_t^0$ and the average decay rate $\Gamma_e$ for PS samples L-1 ($M_w = 8.42 \times 10^6$) and L-2 ($M_w = 20 \times 10^6$) in ETBZ. The translational diffusion coefficients at finite polymer concentrations were determined by fitting the $G^2(\tau)$ data by using the Pike–Ostrowsky multiexponential sampling technique. The infinite dilution translational diffusion coefficient was obtained from

$$\langle D_t\rangle_z = \langle D_t^0\rangle(1 + k_Dc) \quad (21)$$

where $k_D$ can be evaluated by

$$k_D = 1/\langle D_t^0\rangle_z(d\langle D_t\rangle_z/dc)_T \quad (22)$$

and the average hydrodynamic radius $\bar{R}_h$ $(=\langle R_h^{-1}\rangle_z^{-1})$ can be obtained from the Stokes–Einstein equation

$$\langle D_t\rangle_z = kT/6\pi\eta_0\bar{R}_h \quad (23)$$

where $\eta_0$ is the measured solvent viscosity. The experimentally determined parameters were $D_t^0 = 3.3 \times 10^{-8}$ cm$^2$/s, $\bar{R}_h = 1068$ Å, $k_D = 610$ cm$^3$/g for sample L-1 and $D_t^0 = 2.21 \times 10^{-8}$ cm$^2$/s, $\bar{R}_h = 1595$ Å, $k_D = 907$ cm$^3$/g for sample L-2. By way of contrast, in an earlier study of the same samples in THF, we determined $D_t^0 = 4.32 \times 10^{-8}$ cm$^2$/s, $\bar{R}_h = 1086$ Å, $k_D = 1071$ cm$^3$/g for sample L-1 and $D_t^0 = 2.41 \times 10^{-8}$ cm$^2$/s, $\bar{R}_h = 1946$ Å, $k_D = 1510$ cm$^3$/g for sample L-2. It is important to note that for both polymer samples, L-1 and L-2, a bimodal distribution was obtained at the smallest scattering angles ($\theta = 30°$ and 20°, respectively) and hence the $D(c)$ values were computed from the first cumulant of the slow component of $G(\Gamma)$.

The average decay rate $\Gamma_e$ was obtained over a range of concentrations and scattering angles extending to $qR_g \gg$

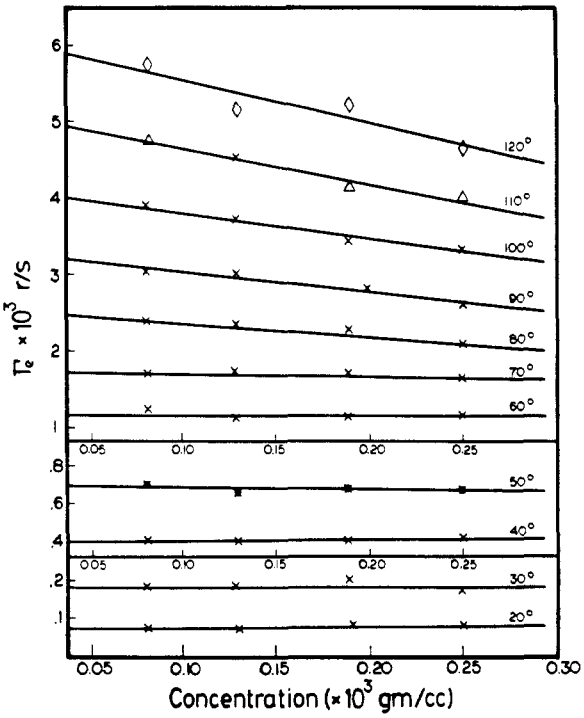


**Figure 5.** $\Gamma_e$ extrapolated to infinite dilution for the sample L-2 at 11 scattering angles from 20° to 120°.

1. Figure 5 shows the concentration dependence of $\Gamma_e(q,c)$ at constant $q$ for the highest molecular weight sample L-2 in ETBZ. The data at each angle are well represented by equations linear in $c$ from which the infinite dilution values $\Gamma_e(q,c=0)$ are estimated. The slopes change sign from positive to negative with increasing $qR_g$ as was observed also for PS in THF.[2] Similar observations have been made independently for PS in benzene[15] and polyisoprenes in cyclohexane[16] in the intermediate $qR_g$ region. The $\Gamma_e(q,c=0)$ results obtained for PS in ETBZ are compared below with our earlier observations for[2] PS in THF and with current theoretical predictions for the behavior of $\Gamma_e$ in the region $qR_g \gg 1$.

## Discussion

Static light scattering data have been obtained for identical polystyrene samples in THF and the aromatic good solvents BZ, TOL, and ETBZ and plotted in a "scaling" form. From this plot it is evident that the intensity data for PS/THF exhibits quite different $(c,q)$-scaling behavior from BZ, ETBZ, and TOL. These observations are consistent with variations noted in the universal ratio $\psi$ for these solvent systems (see Table I). We conclude that in order of decreasing solvent quality, THF > BZ > TOL ≅ ETBZ. This makes doubtful the hypothesis that any of these polymer solvent systems are in the asymptotic excluded volume limit and, particularly, makes doubtful the measured values of $\psi$ and other universal ratios thought to be in this limit.

Turning to our dynamic data for PS in ETBZ, Figure 6 shows the $q^2R_g^2$ dependence of the reduced quantity $\Gamma^{**} = \Gamma_e(q,c=0)/q^2D_t$ in the range $(qR_g)^2 < 40.0$ for the samples L-1 and L-2. For $qR_g \ll 1$ the $\Gamma_e(q,0)$ values are equivalent to $D_t^0q^2$. The increase of $\Gamma_e(q,0)/q^2D_t^0$ with $q$ due to internal motions has been interpreted theoretically at $q^2R_g^2 \gtrsim 1.0$ as

$$\Gamma_e(q,0)/q^2D_t^0 = (1 + C(qR_g)^2 + ...) \qquad (24)$$

and the dimensionless parameter $C$ has been estimated.[13] Theoretical curves of Akcasu and Gurol[43] are shown for

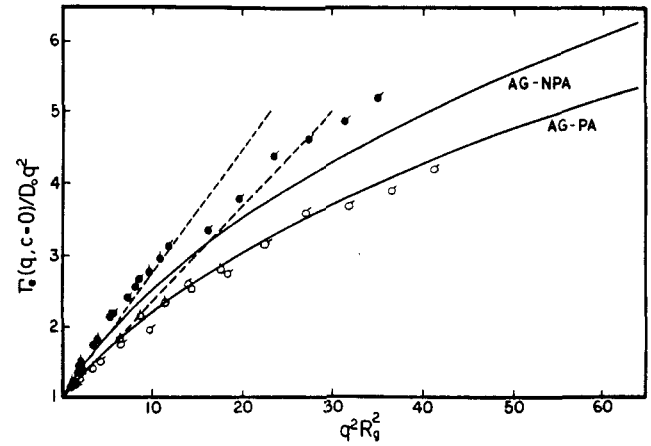


**Figure 6.** Plot of the reduced values $\Gamma_{e,c=0}/q^2D_t$ against $q^2R_g^2$. Shown are the data for PS samples L-1 (○) and L-2 (○) in ETBZ and our previous data for PS in THF (●). The solid lines AG-PA and AG-NPA are the theoretical curves of Akcasu and Gurol (AG)[43] for nondraining Gaussian chains with preaveraged (PA) and non-PA Oseen hydrodynamic interactions, respectively. The broken lines represent the initial slopes, $C = 2/15$ and $C = 13/75$, for the AG-PA and AG-NPA curves, respectively.

Gaussian chains in the nondraining limit by using, respectively, preaveraged (AG-PA) and nonpreaveraged (AG-NPA) hydrodynamic interactions. Clearly, our data for PS in ETBZ are located closer to the theoretical AG-PA curve whose initial slope $C = 0.133$. Figure 6 also show our previous data[2] for PS in THF which behave quite differently and lie close to the AG-NPA curve whose initial slope $C = 0.173$. Similar large differences have been reported by other workers when comparing the good solvent systems PS in BZ[15] and polyisoprene in cyclohexane (PIP/CH).[16] These variations were attributed to the comparative conformational rigidity of the PS chain as compared to polyisoprene. We find that values of $\Gamma^{**}$ for the PS/ETBZ system are in good agreement with the results of Nemoto et al.[15] for the chemically similar system PS/BZ while the values of $\Gamma^*$ for PS in THF are comparable to those of Tsunashima et al. for PIP/CH.[16]

At large scattering angles, $q^2R_g^2 \gg 1.0$, theory predicts[42] that $\Gamma_e$ should scale as $\approx q^3$ for linear flexible chains in the nondraining limit. It is therefore of interest to plot the reduced first cumulant $\Gamma^* = \Gamma_e(q,c=0)/q^3kT/\eta_0$ versus $qR_g$ for PS in ETBZ and compare these with the $\Gamma^*$ values for the PS/THF system. This is shown in Figure 7. Theory predicts that $\Gamma^*(q)$, for long chains, should depend on the intensity of the excluded-volume interaction and hydrodynamic interaction characteristics but that this dependence will tend to zero as the molecular weight increases, provided that the short chain segments have an appreciable excluded-volume and hydrodynamic interaction. In Figure 7, the curves shown again represent various theoretical predictions from the literature. Thus, AG-PA and AG-NPA refer to the fore-mentioned analyses of Akcasu and Gurol[43] for nondraining Gaussian chains using, respectively, preaveraging and nonpreaveraging of the hydrodynamic interactions. Curves BA-PA and BA-NPA indicate the corresponding predictions of Akcasu and Benmouna[44] for the self-avoiding chain limit. Curve OONO represents the RG prediction of Oono et al.[45] for a nondraining self-avoiding chain with nonpreaveraged hydrodynamic interactions. For polystyrene chains, different numerical values of the $\Gamma^*(q)$ asymptote ($\Gamma^*(\infty)$) have been obtained previously for good and Θ solvents in the large $qR_g$ region.[15-17,33,46] The $\Gamma^*$ values obtained in this and in the earlier studies are, however, in disagreement with these theoretical predictions. Thus the analyses of

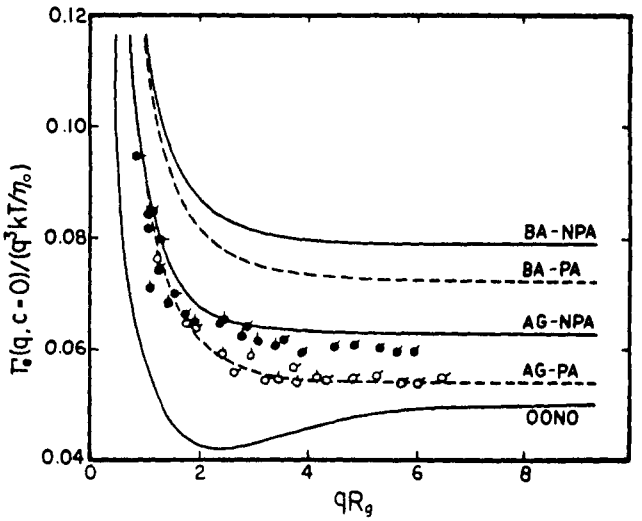


**Figure 7.** Reduced decay rate $\Gamma_e(q,0)/q^3kT/\eta_0$ as a function of $qR_g$. Symbols are the same as in Figure 6. The solid lines AG-NPA[43] and BA-NPA[44] represent the theoretical curves for nondraining chains in the θ- and good-solvent limits from nonpreaveraged Oseen hydrodynamics. AG-PA and BA-PA correspond to similar calculations using a preaveraged Oseen tensor. The solid line OONO[45] is for self-avoiding chains with the non-PA Oseen tensor.

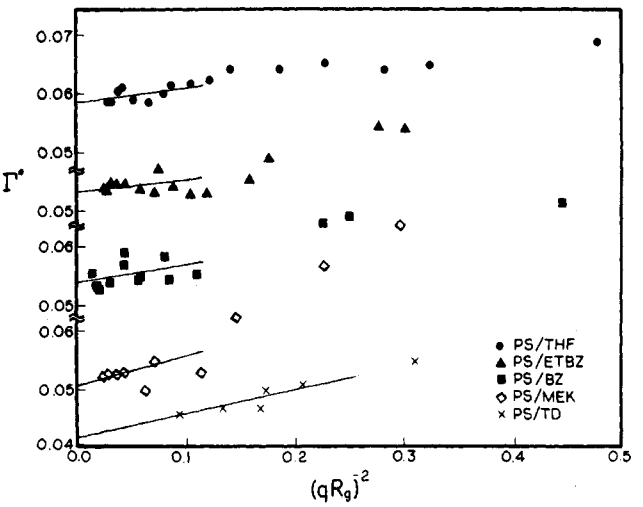


**Figure 8.** Plot of the reduced values Γ* versus $1/q^2R_g^2$. Shown are the data for PS/THF, PS/ETBZ, PS/BZ,[15] PS/*trans*-decalin,[39] and PS/MEK.[24]

Benmouna and Akcasu (BA)[44] for good solvents overestimate Γ*(∞) while the Oono prediction of Γ*(∞) is too small. In fact, Γ* data for swollen chains consistently fall closer to the Akcasu–Gurol analyses for Gaussian chains, while experimental Γ*(q) data in θ solvents approach an asymptote substantially smaller than the AG predictions. Currently there are no explanations for the above deviations. It is clear from Figure 7 that our Γ* data for PS in ETBZ and PS in THF are likewise in disagreement with theoretical expectation. In each solvent, the Γ* values for different molecular weights superpose on a master curve which decreases rapidly for $qR_g < 2$ and approaches an asymptote in the range $qR_g \cong 4$. However, our experimental asymptote for PS in ETBZ lies close to the AG-PA prediction for Gaussian chains with preaveraged Oseen hydrodynamic interactions while our earlier results for Γ* in PS in THF approach an asymptote which is considerably larger than that predicted by the AG-PA theory and, in fact, is close to the AG-NPA asymptote. We note that our Γ* data for PS/ETBZ are consistent with the data of Nemoto et al.[15] for PS in BZ while our Γ* values for PS in THF are similar to those observed by Tsunashima et al.[16] for highly swollen polyisoprene chains. Evidently, the Γ* and Γ** quantities confirm that there are indeed differences between the dynamical properties of PS in THF and in ETBZ. Since theoretical models are unable to rationalize the observed data, it is not possible to unambiguously assign these differences to variations in the excluded-volume chain conformation and/or hydrodynamic interaction.

Because Γ* slowly varies in the large $qR_g$ region, it is evident that a more precise method of estimating the asymptotic value of Γ* would be useful. Previously, many graphical analyses[46,47] of data for Γ* have consisted of plotting Γ* as a function of the static parameter $qR_g$ and extrapolating the roughly hyperbolic curves to infinite $qR_g$. A more useful procedure is to plot Γ* as a function of $(qR_g)^{-2}$. Theoretical analysis based on the renormalization group suggests that for intermediate $qR_g$, Γ* should be approximately linear in $(qR_g)^{-2}$, although this approximation is expected to break down both for very large $qR_g$ where Γ* behaves as the difference of two similar but smaller powers and for small $qR_g$. We anticipate therefore that these plots of Γ* versus $(qR_g)^{-2}$ would be roughly linear at least for the intermediate range of wavevectors we have probed, provided that the system is not crossing over from one behavior to another, e.g., from nondraining to free-draining hydrodynamics or from Gaussian to self-avoiding statistics. Hence, in Figure 8, we plot our data in the above form for PS in THF, ETBZ, and other solvent systems. The approximate linearity of these curves for large $qR_g$ confirms the theoretical prediction and the utility of this method of plotting the data. It is clear that a range of different asymptotes is observed for the various solvent systems. From the previous experimental evidence it appears that this variation is due to a variety of solvent-specific behaviors including changes in local microstructure, excluded-volume, and hydrodynamic interactions.

In conclusion, we find that the static light scattering properties of dilute polystyrene solutions in the aromatic good solvents BZ, ETBZ, and TOL are different from those in the polar solvent THF. As a working hypothesis we suggest that in THF, PS has a substantially more flexible microstructure, but at the same time, PS is more strongly solvated and hence is closer to the asymptotic good-solvent limit. The dynamic light scattering properties of dilute PS solutions in ETBZ extending from the small to the intermediate $qR_g$ region are also different from those in THF. At $qR_g \ll 1$, we find that the ratio of $R_h$ to $R_g$ is larger for PS in THF than for PS in ETBZ. We have previously interpreted this effect as indicative of a comparatively smaller draining effect in THF. At $qR_g \gg 1$, experimental values of the reduced decay rate Γ* again show substantial differences when comparing PS in THF and in ETBZ. These effects cannot be interpreted on the basis of any of the currently available theoretical models. We have proposed a new graphical analysis to estimate more precisely the value of the Γ* asymptote. A survey of available data suggests a variety of nonuniversal dynamical properties. To fully understand current experimental observations regarding the discrepancies between PS/ETBZ and PS/THF, the current hydrodynamic theory will probably need to be modified to include phenomena such as internal friction, chain rigidity, variations in the degree of draining, and/or hydrodynamic screening.

**Acknowledgment.** We thank the Materials Research Laboratory for support of this work through research award NSF DMR 86-14093.

**Registry No.** PS, 9003-53-6.

## References and Notes


(1) Venkataswamy, K.; Jamieson, A. M. *Macromolecules* **1986**, *19*, 124.
(2) Bhatt, M.; Jamieson, A. M. *Macromolecules* **1988**, *21*, 3015.
(3) Jamieson, A. M.; Venkataswamy, K. *Polym. Bull. (Berlin)* **1984**, *12*, 275.
(4) Miyaki, Y.; Einage, Y.; Fujita, H. *Macromolecules* **1978**, *11*, 1180.
(5) Adam, M.; Delsanti, M. *Macromolecules* **1977**, *10*, 1229. de Gennes, P.-G. *Phys. Lett.* **1972**, *38A*, 339. *Scaling Concepts in Polymer Physics*; Cornell University Press: Ithaca, NY, 1979.
(6) Fukuda, M.; Fukutomi, F.; Kato, Y.; Hashimoto, M. *J. Polym. Sci., Polym. Phys. Ed.* **1974**, *12*, 871.
(7) Appelt, B.; Meyerhoff, G. *Macromolecules* **1980**, *13*, 657.
(8) Utiyama, H.; Utsumi, H.; Tsunashima, Y.; Kurata, M. *Macromolecules* **1978**, *11*, 506.
(9) Mandema, W.; Zeldenrust, H. *Polymer* **1977**, *18*, 835.
(10) McDonnell, M. E.; Ramanathan, M. *Macromolecules* **1984**, *17*, 2093.
(11) McDonnell, M. E.; Jamieson, A. M. *J. Macromol. Sci., Phys.* **1977**, *B13*, 67.
(12) Yu, T. L.; Reihanian, H.; Jamieson, A. M. *Macromolecules* **1980**, *13*, 1590.
(13) Burchard, W.; Schmidt, M.; Stockmayer, W. H. *Macromolecules* **1980**, *13*, 580.
(14) Koppel, D. E. *J. Chem. Phys.* **1972**, *57*, 4814.
(15) Nemoto, N.; Makita, Y.; Tsunashima, Y.; Kurata, M. *Macromolecules* **1984**, *17*, 425.
(16) Tsunashima, Y.; Hirata, M.; Nemoto, N.; Kurata, M. *Macromolecules* **1987**, *20*, 1992.
(17) Wiltzius, P.; Haller, H. R.; Cannell, D. S.; Cannell, D. W. *Phys. Rev. Lett.* **1983**, *51*, 1183.
(18) Oono, Y.; Kohomoto, M. *J. Chem. Phys.* **1983**, *78*, 520.
(19) Oono, Y. *Adv. Chem. Ser.* **1987**, 1.
(20) Zimm, B. H. *Macromolecules* **1980**, *13*, 592.
(21) Fixman, M. *J. Chem. Phys.* **1986**, *84*, 4085.
(22) Douglas, J. F.; Freed, K. F. *Macromolecules* **1984**, *17*, 2354.
(23) (a) Douglas, J. F.; Freed, K. F. *Macromolecules* **1984**, *17*, 2344. (b) Freed, K. F.; Douglas, J. F.; Wang, S. Q.; Perico, A. *Polymer-Flow Interaction*; AIP Conference Proceedings 137; American Institute of Physics: New York, 1985.
(24) Wiltzius, P.; Cannell, D. S. *Phys. Rev. Lett.* **1986**, *56*(1), 61.
(25) Spychaj, T.; Lath, D.; Berek, D. *Polymer* **1979**, *20*, 437.
(26) Zimm, B. H. *J. Chem. Phys.* **1948**, *16*, 1099.
(27) Berry, G. C. *J. Chem. Phys.* **1966**, *44*, 12, 4550.
(28) Ostrowsky, N.; Sornette, D.; Parker, P.; Pike, E. R. *Opt. Acta* **1981**, *28*, 1059.
(29) McWhirter, J. G.; Pike, E. R. *J. Phys. A: Math Gen.* **1978**, *11*, 1729.
(30) Dahneke, B. E. *Measurement of Suspended Particles by QELS*; Wiley: New York, 1983; pp 107–127.
(31) McWhirter, J. G. *Opt. Acta* **1980**, *27*, 83.
(32) Pike, E. R.; Pomeroy, W. R.; Vaughan, J. M. *J. Chem. Phys.* **1975**, *62*, 3188.
(33) Han, C. C.; Akcasu, A. Z. *Macromolecules* **1981**, *14*, 1080.
(34) Hendrix, J.; Saleh, B. *Polymer* **1977**, *18*, 10. Freire, J. J. *Polymer* **1978**, *19*, 1441.
(35) Gulari, E.; Gulari, E.; Tsunashima, Y.; Chu, B. *J. Chem. Phys.* **1979**, *70*, 3965.
(36) Gulari, E.; Gulari, E.; Tsunashima, Y.; Chu, B. *Polymer* **1979**, *20*, 347.
(37) Nose, T.; Chu, B. *Macromolecules* **1979**, *12*, 1122.
(38) Tsunashima, Y.; Hirata, M.; Nemoto, N.; Kurata, M. *Macromolecules* **1983**, *16*, 584.
(39) Tsunashima, Y.; Nemoto, N.; Kurata, M. *Macromolecules* **1983**, *16*, 1184.
(40) Chu, B.; Wu, D. Q. *Macromolecules* **1987**, *20*, 1606.
(41) Provencher, S. W. *J. Chem. Phys.* **1976**, *64*, 2772.
(42) Dubois-Voilette, E.; de Gennes, P.-G. *Physics (Long Island City, N.Y.)* **1967**, *3*, 181.
(43) Akcasu, A. Z.; Gurol, H. J. *J. Polym. Sci., Polym. Phys. Ed.* **1976**, *14*, 1. Akcasu, A. Z.; Han, C. C.; Benmouna, M. *Polymer* **1980**, *21*, 866.
(44) Benmouna, M.; Akcasu, A. Z. *Macromolecules* **1980**, *13*, 409. Benmouna, M.; Akcasu, A. Z. *Macromolecules* **1978**, *11*, 1187.
(45) Lee, A.; Baldwin, P. R.; Oono, Y. *Phys. Rev. A* **1984**, *30*(2), 968.
(46) Tsunashima, Y.; Hirata, M.; Nemoto, N.; Kanjiwara, K.; Kurata, M. *Macromolecules* **1987**, *20*, 2862.
(47) Stockmayer, W. H.; Hammouda, B. *Pure Appl. Chem.* **1984**, *56*(10), 1373.
(48) Fujita, H. *Macromolecules* **1988**, *21*, 179.
(49) Fujita, H.; Norisuye, T. *Macromolecules* **1985**, *18*, 1637.
(50) Huber, K.; Bantle, S.; Lutz, P.; Burchard, W. *Macromolecules* **1985**, *18*, 1461.
(51) Huber, K.; Stockmayer, W. H. *Macromolecules* **1987**, *20*, 1400.
(52) Benoit, H.; Benmouna, M. *Polymer* **1984**, *25*, 1059.
(53) Fujita, H. *Polym. J.* **1970**, *1*, 537.
(54) Ohta, T.; Oono, Y. *Phys. Lett.* **1982**, *89A*, 460.


# An Insight into the Barton Equation for Copolymer Glass Transition


**Hidematsu Suzuki***

*Institute for Chemical Research, Kyoto University, Uji, Kyoto-Fu 611, Japan*

**V. B. F. Mathot**

*DSM Research and Patents, P.O. Box 18, 6160MD Geleen, The Netherlands.*

*Received April 20, 1988; Revised Manuscript Received August 2, 1988*


ABSTRACT: New expressions of the Barton equation for the copolymer glass transition temperature $T_g$ are derived to make its potential characteristics clear. On a plot of $T_g$ against the run number $R$ instead of composition, (i) the arithmetic mean of the homopolymer $T_g$ values, the $T_g$ of the equimolar random copolymer, and the $T_g$ of the corresponding alternating copolymer are on the same straight line and (ii) $T_g$ values of two random copolymers having a given value of $R$, but different compositions, deviate equally from the line mentioned above. Applications of the new expressions to three different typical data in the literature are illustrated as demonstrations of potentials of the equations.


## Introduction

As is well-known, the glass transition temperatures of copolymers deviate from linear relations such as the DiMarzio–Gibbs equation[1]

$$T_g = m_A T_{gA} + m_B T_{gB} \quad (1)$$

Here, $T_g$ is the glass transition temperature of a copolymer composed of two monomer units A and B with mole fractions $m_A$ and $m_B$, and $T_{gA}$ and $T_{gB}$ are, respectively, the $T_g$ values of the homopolymers of A and B. The failure, in predicting $T_g$ values, of linear relations including the reciprocal expression like the Fox equation[2] represents

0024-9297/89/2222-1380$01.50/0 